Journal of Control, Automation and Electrical Systems (2019) 30:1082–1093
https://doi.org/10.1007/s40313-019-00500-y

A Real-Time Synchronized Harmonic Phasor Measurements-Based Fault Location Method for Transmission Lines

Balimidi Mallikarjuna[1] · Gopakumar Pathirikkat[2] · Diptendu Sinha Roy[3] · Jaya Bharata Reddy Maddikara[1]

Received: 8 November 2018 / Revised: 4 May 2019 / Accepted: 18 July 2019 / Published online: 31 July 2019

Abstract

In this paper, a real-time synchronized harmonic phasor measurements-based fault location (RT-SHPM-FL) method for transmission lines is proposed. At transmission line protection center (TPC), the synchronized harmonic phasor measurements are obtained from all phasor measurement units (PMU) deployed in a power system. At each bus, the PMU estimates time-tagged 100 and 150 Hz phasors of 3-ϕ current signals in addition to fundamental phasor (50 Hz). The proposed RT-SHPM-FL method detects and locates a fault using the magnitude of 100 and 150 Hz phasors of 3-ϕ currents and equivalent harmonic phasors (EHPs), respectively. These EHPs are calculated from the magnitude of time-tagged 50, 100 and 150 Hz three-phase current phasors. For estimating the fault distance, the RT-SHPM-FL method has employed support vector regression (SVR), because of its mimicking nature, generalization and robustness. The functioning of the proposed fault location method has been validated in real-time on a scaled-down laboratory model of 400 kV extra high voltage (EHV) transmission line of 400 km long. The experimental results and discussions show that the proposed method locates transmission line faults accurately. Further, a comparative study of the proposed fault location method using SVR and adaptive neuro-fuzzy inference system has revealed that the former one is more reliable in fault location than the latter one since the error is within $\pm 1\%$.

Keywords Synchrophasors · Phasor measurement unit (PMU) · Support vector regression (SVR) · Adaptive neuro-fuzzy inference system (ANFIS)

Abbreviation

RT-SHPM-FL	Real-time synchronized harmonic phasor measurements-based fault location
LabVIEW	Laboratory virtual instrument engineering workbench
NI cRIO	National instruments compact reconfigurable input/output embedded controller
SVR-FL	Support vector regression fault location
ANN	Artificial neural network
ANFIS	Adaptive neuro-fuzzy inference system
$x(t)$	Analog voltage or current signal
$x(n\Delta T)$	Sampled version of $x(t)$
ΔT	Sampling time in seconds
T	Nominal time in seconds
f_o	Nominal frequency (Hz)
N	Number of samples per cycle
n	Sample number starting (0 to $N-1$)
$h=1$	Fundamental frequency phasor of line current
$h=2$	Second-order harmonic phasor of line current

Electronic supplementary material The online version of this article (https://doi.org/10.1007/s40313-019-00500-y) contains supplementary material, which is available to authorized users.

✉ Balimidi Mallikarjuna
arjun.malli4@gmail.com

Gopakumar Pathirikkat
gopuvattekkat@gmail.com

Diptendu Sinha Roy
diptendu.sr@nitm.ac.in

Jaya Bharata Reddy Maddikara
jayabharat_res@yahoo.co.in

[1] Department of EEE, National Institute of Technology, Tiruchirappalli, Tiruchirappalli, Tamil Nadu 620015, India

[2] Department of Electrical Engineering, National Institute of Technology, Calicut, Calicut, Kerala 673601, India

[3] Department of Computer Science and Engineering, National Institute of Technology, Meghalaya, Shillong 793003, India

$h=3$	Third-order harmonic phasor of line current
$\langle , \rangle$	Dot product in R^n
C	Pre-specified value
β_i	Loss functions
γ_i	Slack variables

1 Introduction

Transmission lines are the veins of power system, which carry bulk amount of energy from generating stations to consumers through different terrains under various environmental conditions. Hence, they are likely to be exposed to various power system disturbances, which can spread to a larger extent of the grid. These disturbances may render the power supply unreliable and unstable. In this regard, the perception of transmission line protection philosophy has been changing from local to wide area. Newer technologies are being incorporated into the existing power system to effectively protect the power grid from disturbances. One of the most important technologies in wide-area protection philosophy is synchrophasor measurements. Incorporation of such technology into the transmission line protection reduces the impact of catastrophic events on the performance of power system infrastructure and also improves the situational awareness.

Some of the methodologies based on synchrophasor technology for transmission line protection have been discussed here. Jiang et al. (2012) have proposed an effective fault location method using the optimal measurements and distributed parameter line model. Mousavi-Seyedi et al. (2015) proposed a fault location algorithm for series-compensated transmission lines. Vallapu et al. (2017) have employed an event-driven communication strategy for data communication with the centralized controller to detect and locate a transmission line fault. Kang et al. (2017) have presented a novel fault location algorithm for two-end series-compensated double-circuit transmission line. The fault location methodology has employed two unsynchronized terminal current and local voltage phasors for accurate fault location. Further, Das et al. (2017) have designed a fault location method for transmission lines using only voltage phasors and admittance matrix. The algorithm is less sensitive to fault inception angles (FIA), fault types and fault resistances (FR). However, the accuracy of the proposed fault location algorithms (Jiang et al. 2012; Das et al. 2017; Kang et al. 2017) depends on the distributed line parameters.

Further, Saber (2018) has proposed a novel algorithm for the location of a fault in two-terminal transmission lines. The method is less sensitive to FIA, fault types, FR, variation in soil resistivity, measurement and line parameters error, etc. Barman and Roy (2018) have employed phasor measurements obtained from optimally placed PMUs for fault detection and location. Location of the fault has been identified by linearizing nonlinear set of voltage and current equations using least square estimation problem. Meenakshi Devi et al. (2018) have proposed a novel fault location algorithm using the latitude and longitude by involving georeferenced data of the power system. Rajaraman et al. (2018) have proposed a robust fault analysis algorithm for transmission line protection. The methodology has determined the sequence components from voltage and current phasors to detect, classify and locate the fault. Mallikarjua et al. (2018) have proposed fault detection and classification methodology using time-tagged predominant harmonic phasors of current signals. It has been implemented in real time on the scaled-down laboratory models. However, the proposed methodology is limited to fault detection and classification only.

Furthermore, advancement in artificial intelligence has facilitated many applications in power system protection due to their mimicking nature, generalization and robustness. Gao et al. (2015) have put forward a nonparametric technique-based fault classification method for transmission lines. The proposed technique has used voltage phasors. Roy and Bhattacharya (2015) have proposed multi-resolution S-transform-based methodology for transmission lines protection from all types of faults. It has employed probabilistic neural networks for fault detection and classification. The probabilistic neural networks have been trained with the features extracted from current signals. Manassero Junior et al. (2016) have proposed a fault location methodology for series-compensated transmission lines. In this context, it has utilized voltage and current phase components along with the heuristic method. The proposed method is developed on the assumption that no errors are present in the transmission line parameters estimation. Most of these methods (Jiang et al. 2012; Mousavi-Seyedi et al. 2015; Vallapu et al. 2017; Kang et al. 2017; Das et al. 2017; Saber 2018; Barman and Roy 2018; Meenakshi Devi et al. 2018; Rajaraman et al. 2018) discussed above are confined to simulation based validations only.

In (Venkatesan and Balamurugan 2001), real-time fault detector based on artificial neural networks (ANNs) was developed for the protection of transmission lines. In this system, voltage and current signals before and after fault are employed for fault location. Pasand and Malik (1999) have realized ANN-based directional distance protection algorithm using analog-to-digital (A/D) converter in conjunction with DSP processor (TMS320C30 DSP chip). However, the methodology is constrained to detection of fault direction only. For achieving precise fault location using synchrophasor measurements, support vector machine (SVM) has been employed (Gopakumar et al. 2015; Jaya Bharata Reddy et al. 2016) since it is superior over ANFIS (Kumar et al. 2015) and ANN (Venkatesan and Balamurugan 2001; Pasand and

Malik 1999) in generalization and robust in handling multi-dimensional data. Gopakumar et al. (2015) proposed an SVM-based fault detection and classification methodology. The methodology has employed harmonic components of equivalent voltage and current phasor angles. Jaya Bharata Reddy et al. (2016) have developed a smart methodology for detection, classification and location of transmission lines faults using discrete orthogonal Stockwell transform (DOST). The fault detection and classification functions are accomplished using synchronized current measurements obtained from remote terminal units (RTUs) at both ends of a transmission line, and faults are located using SVM.

The noteworthy contribution of the proposed RT-SHPM-FL method is that it locates a fault accurately using SVR, and this information is useful to restore the faulted line at the earliest. It has been implemented on a scaled-down laboratory model of the 400 kV transmission line using EHPs calculated from the magnitudes of time-tagged fundamental, second- and third-order harmonic phasors of three-phase currents. A PMU has been realized using NI cRIO-9063 chassis, NI-9227 current sensor card, NI-9467 GPS module and LabVIEW software. The experimental results show that the proposed fault location method locates the fault precisely. Furthermore, a comparative study reveals that the proposed method using SVR is more accurate than ANFIS because the error associated with the former is within $\pm 1\%$.

2 Proposed RT-SHPM-FL Method

Accurate location of a fault in transmission lines is a necessary task to guide the crew for restoring the power supply at the earliest. For such applications, the combination of synchrophasor measurements and machine learning techniques such as ANN, ANFIS and SVR are promising technologies. In this paper, the proposed RT-SHPM-FL method employs synchronized current phasor data and SVR for fault location. In order to understand the proposed method, the technical background of synchrophasor technology and SVR is essential.

2.1 Synchrophasor Technology

The vanguard synchrophasor technology estimates the time-tagged phasor measurements w.r.t the time reference of Global Positioning System (GPS). In a PMU as shown in Fig. 1, the phasor estimation process starts with a sampling of an analog signal at a sampling frequency ($f_s = Nf_o$). The time-tagged f_o, $2f_o$ and $3f_o$ harmonic phasors of each phase of three-phase current signals are estimated per cycle using a discrete Fourier transform (DFT) algorithm as given in Eq. (1). DFT requires N

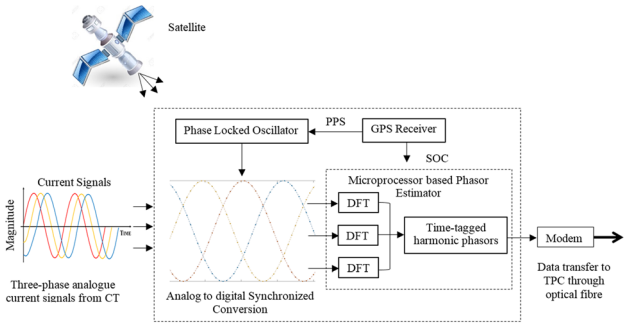

Fig. 1 Block diagram of phasor measurement unit (PMU)

number of samples per cycle. The hth harmonic phasor estimation of an original signal is given by

$$X_h = \frac{\sqrt{2}}{N} \sum_{n=0}^{N-1} x(n\Delta T) e^{-j\frac{2\pi hn}{N}} \tag{1}$$

The synchronized measurements from PMUs are transmitted over the TCP/IP protocol between the PMU and the phasor data concentrator (PDC) at transmission line protection center (TPC) as per the synchrophasor standard C37.118.2 [IEEE Standard for Synchrophasor Data Transfer for Power Systems].

2.2 Support Vector Regression

The classical problem associated with statistical learning theory and structural risk minimization can be solved using SVM Vapnik 1998). As stated by Vapnik et al. (1997), SVMs can also be employed for regression problems using an alternative loss function, though they have been used for fault type identification and estimation of transmission line parameters for fault locations. These SVMs are named as SVR. For real value inputs, SVR predicts a real value output. SVR is classified as either linear or nonlinear SVRs. The fault location function has been implemented in MATLAB environment with LIBSVM toolbox (Chang and Lin 2011) for SVR training and testing. Further, the estimated fault distance is displayed in LabVIEW front panel through LabVIEW and MATLAB interface.

Consider a set of data (x_i, y_i) to be trained, $x_i \in R^n$, $y_i \in R$, where $i = 1, 2 \ldots l$. x_i represents the input data and y_i implies the output data. Linear SVR is performed on the data, which is mapped into high-dimensional feature space where a nonlinear mapping Φ is sought.

Let us take a linear function with a mapping Φ:

$$f(x) = \langle \omega, \Phi(x) \rangle + b \tag{2}$$

The optimal regression function is obtained from the minimum of Eq. (3):

$$R(\omega, b, \gamma, \gamma^*) = \frac{1}{2}\|\omega\|^2 + C\sum_{i=1}^{l}(\beta_i(\gamma_i) + \beta_i(\gamma_i^*) \quad (3)$$

The SVR problem can be redefined as finding an optimal solution to the following quadratic programming problem based on Eqs. (4) and (5):

Objective function:

$$\min R(\omega, b, \gamma, \gamma^*) = \frac{1}{2}\|\omega\|^2 + C\sum_{i=1}^{l}(\beta_i(\gamma_i) + \beta_i(\gamma_i^*)\left\langle \omega, \dot{\Phi}(x)\right\rangle + b - y_i \le \gamma_i + \epsilon \quad (4)$$

$$\text{Subject to } y_i - \left\langle \omega, \dot{\Phi}(x)\right\rangle - b \le \gamma_i + \epsilon\gamma_i,\ \gamma_i^* \le 0$$

The solution of quadratic programming problem is easily obtained by proposing a dual set of variables a_i and a_i*. A Lagrange-like function is formed using the objective function and the corresponding constraints with few mathematical manipulations as given below (Fei et al. 2018; Yusuff et al. 2014):

$$\max W(a, a^*, \gamma, \gamma^*) = \frac{1}{2}\sum_{i,j=1}^{l}(a_i - a_i^*)\left(a_j - a_j^*\right)\left\langle \Phi(x_i), \Phi(x_j)\right\rangle + \sum_{i=1}^{l}(a_i^* - a_i)y_i - \epsilon\sum_{i=1}^{l}(a_i - a_i^*) + C\sum_{i=1}^{l}(\beta_i(\gamma_i) + \beta_i(\gamma_i^*)) - \gamma_i\frac{d}{d\gamma_i}\beta_i(\gamma_i) - \gamma_i^*\frac{d}{d\gamma_i^*}\beta_i(\gamma_i^*) \quad (5)$$

The mapping of input space with the output space is in general nonlinear. For achieving a better mapping in a high-dimensional feature space, Kernel functions $K(X_i, X_j)$ are used in computing a dot product. Frequently used kernels in most of the applications are the linear kernel, polynomial kernel, radial basis kernel (RBK) and sigmoidal kernel. For realizing a nonlinear mapping, the quadratic loss function $\beta(\gamma) = \gamma^2$ and RBK, as given by Eq. (6), are selected:

$$K(X, X_i) = e^{-(\|X - X_i\|^2)/2\sigma^2} \quad (6)$$

Thus, optimization problem for SVR is changed to

$$\max W(a, a^*) = \frac{1}{2}\sum_{i,j=1}^{l}(a_i - a_i^*)\left(a_j - a_j^*\right)K(X, X_i) + \sum_{i=1}^{l}(a_i^* - a_i)y_i - \frac{1}{2C}\sum_{i=1}^{l}(a_i^2 - a_i^{*2}) \quad (7)$$

subject to $\sum_{i=1}^{l}(a_i^* - a_i) = 0$; a_i and $a_i^* \in [0, C]$.

2.3 Flowchart of the Proposed RT-SHPM-FL Method

Step 1 Synchronized time-tagged harmonic phasors of 3-ϕ signals estimated by PMU are received at TPC and plot 3-ϕ and individual phase current signals as shown in Fig. 2

Step 2 If second-order ($I_{p2} = 100$ Hz) and third-order ($I_{p3} = 150$ Hz) harmonic current phasors are greater than the respective threshold value (k_1 & k_2), a fault is detected. Else 'No fault', and hence, go to Step 1

Step 3 The magnitude of EHPs (I_{eq1}, I_{eq2} and I_{eq3}) is calculated from the magnitude of 50, 100 and 150 Hz three-phase current phasors using Eqs. (8)–(10) (Mallikarjua et al. 2018)

$$|I_{eq1}| = \sqrt{|I_{A1}|^2 + |I_{B1}|^2 + |I_{C1}|^2} \quad (8)$$

$$|I_{eq2}| = \sqrt{|I_{A2}|^2 + |I_{B2}|^2 + |I_{C2}|^2} \quad (9)$$

$$|I_{eq3}| = \sqrt{|I_{A3}|^2 + |I_{B3}|^2 + |I_{C3}|^2} \quad (10)$$

Step 4 A nonlinear SVR as given in Eq. (7) is trained with the magnitude of EHPs ($I_{eq1}, I_{eq2}\&I_{eq3}$) regarding different faults with various fault conditions as input data and fault distance (in km) as output data

Step 5 Send $|I_{eq1}|$, $|I_{eq2}|$ and $|I_{eq3}|$ of new fault condition through the trained fault location function (SVR-FL) of RT-SHPM-FL method to estimate the actual fault distance in 'km'

A brief description of the experimental setup for implementing the RT-SHPM-FL method in real-time is given in the succeeding section.

3 Description of Experimental Setup

Details of the major components of the experimental setup are given in the subsequent sections.

3.1 Three-Phase Power Supply, EHV Transmission Line and Variable Load

As shown in Fig. 3, scaled-down laboratory prototype of 400 kV extra high voltage (EHV) transmission line of 400 km is connected between a 3-Φ, 440 V (L–L), 50 Hz power supply and an autotransformer of 440 V to (0–110 V), 50 Hz. The three-phase voltage and current signals can be measured from the tapping on the laboratory model. It has been divided into eight 50-km Π-sections. At every 50 km,

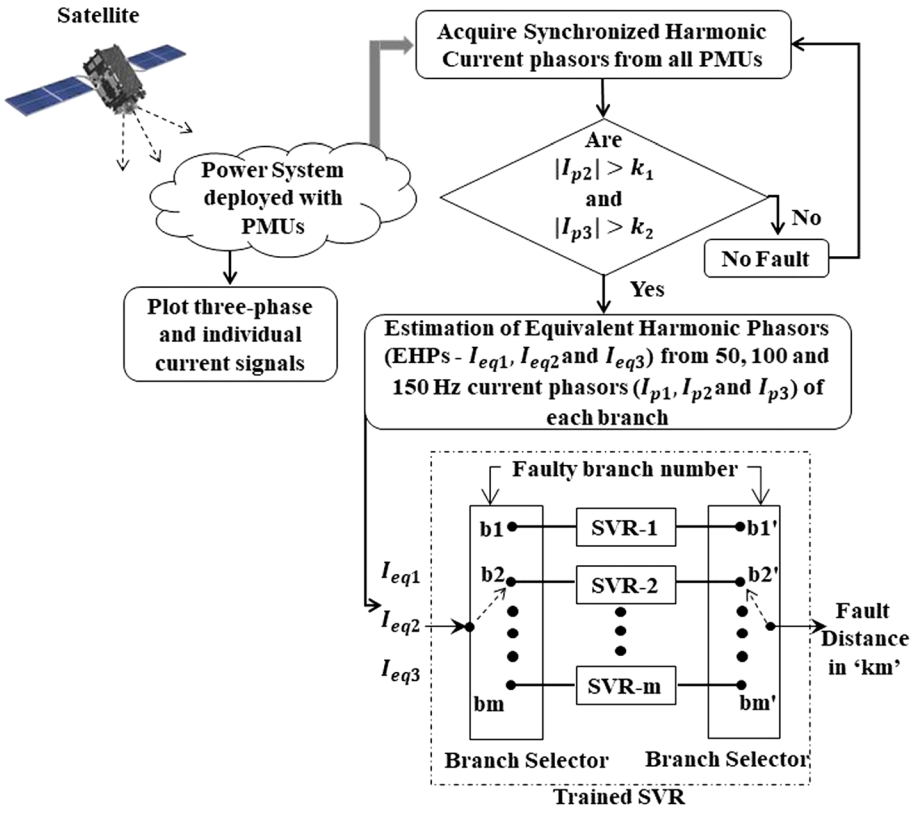

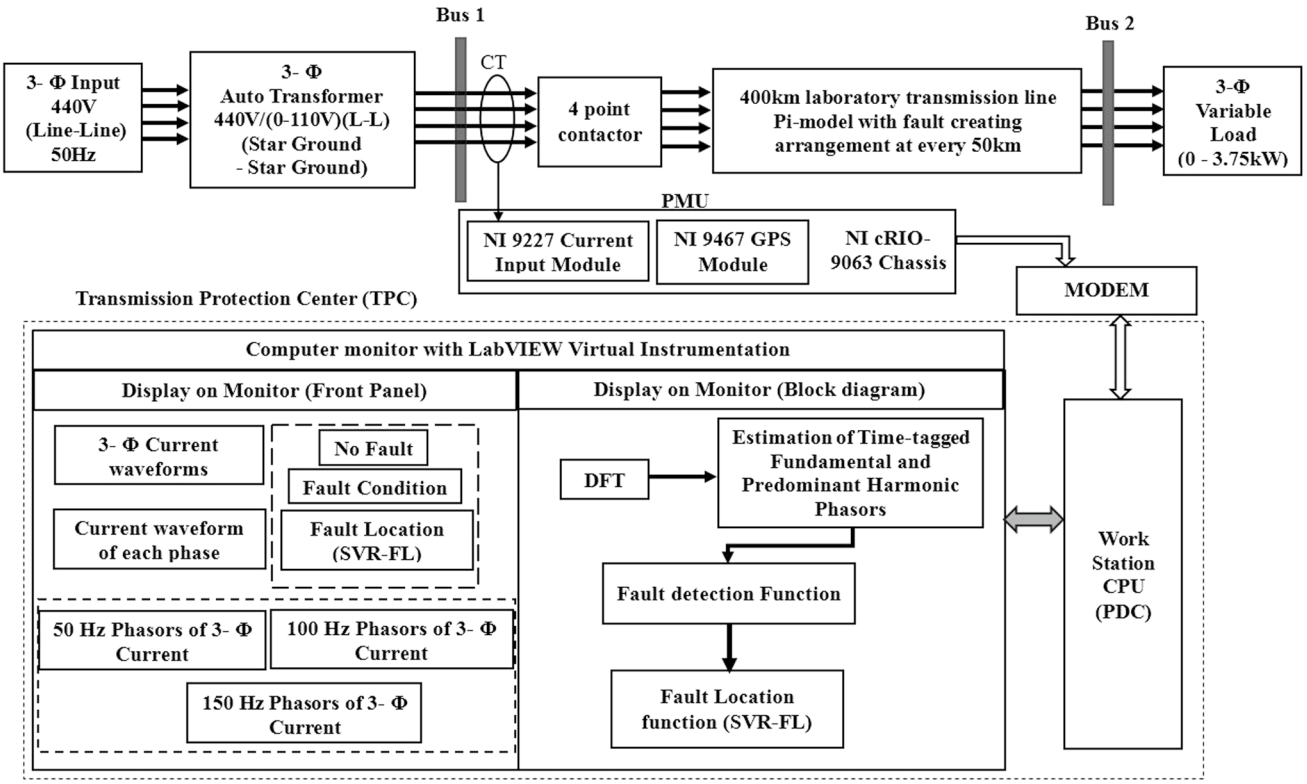

Fig. 2 Implementation of a generalized RT-SHPM-FL method using SVR at TPC

Fig. 3 Scaled-down laboratory model of EHV transmission system connected with PMU and execution of the proposed fault location method in LabVIEW at TPC

ports have been provided to create an external disturbance. The resistance, inductance and capacitance of the transmission line are 0.036 Ω/km, 0.2014 mH/km and 0.044 μF/km, respectively. A 4-pole contactor acts as a circuit breaker. The three-phase variable load of 1.25 kW/phase is connected at the transmission line's receiving end.

3.2 Realization of PMU

Real-time implementation of PMU for harmonic phasor estimation has been done using a fast, efficient and reliable NI cRIO-9063 chassis embedded with data acquisition (NI 9227 current) and time stamping (NI 9467 GPS) modules in conjunction with LabVIEW FPGA software. The NI devices have been chosen because they are extremely compact in size, rugged in construction, reliable and flexible for input/output connection. Also, they can function reliably in −40 to 70 °C temperature range.

3.2.1 cRIO-9063 (Chassis)

The NI cRIO devices offer powerful stand-alone and also networked execution for real-time deterministic applications. A reconfigurable FPGA of cRIO facilitates custom timing, triggering and processing. It is embedded with a 667 MHz dual-core ARM Cortex-A9 processor and 4-slot Artix-7 FPGA. It contains dynamic RAM of 256 MB for embedded operation and 512 MB nonvolatile memory for data logging. It has been supplied through a power module which can provide an isolated voltage of range 9–30 V.

3.2.2 Current Module: NI 9227

The NI 9227 current module is interleaved in cRIO chassis for acquiring the current samples. It is designed to measure current signals of 5 A r.m.s. nominal current. It can sustain the current up to 14 A peak current on each channel with channel-to-channel isolation. It contains four distinct channels. The maximum sampling speed of the device is 50 kS/s per channel.

3.2.3 GPS Module: NI 9467

The NI 9467 GPS module is selected for obtaining accurate time stamping, system clock setting and geographic location information based on pulse per second (PPS) signal arrival from the satellite. The NI FPGA timekeeper is designed to integrate the cRIO onboard FPGA clock with external timing sources such as SNTP, IRIG-B and GPS. The combination of NI 9467 and NI FPGA timekeeper provides time stamps each at a tick of 0.025/0.0125 μ second clock with real-world time, which is accurate to within ± 100 ns.

3.2.4 NI LabVIEW FPGA

The graphical development for FPGA chips on NI cRIO hardware target has been done using the LabVIEW FPGA Module. The graphical code in the form of virtual instrumentation (VI) can be compiled and implemented in hardware with the LabVIEW FPGA Module on a host computer. The custom hardware-based user-defined logic can also be created using FPGA VIs for many applications like digital protocol communication, hardware-in-the-loop (HIL) simulation, etc. Since FPGA module has many built-in signal processing routines, it is possible to integrate existing hardware description language (HDL) code as well as third-party IP including Xilinx CORE Generator functions. The important feature of LabVIEW FPGA module is that the graphical code will be automatically converted into VHDL code and that will be converted into bit file using Xilinx ISE compiler.

The PMU (cRIO-9063 embedded with the NI-9227 current sensor card and NI-9476 GPS) is connected as shown in Fig. 3. The cRIO chassis acquires the digital form of the analog three-phase current signals through the current sensor card. These measurements are transferred to the central processing unit (CPU) of the personal computer (PC) where LabVIEW FPGA software estimates the time-tagged fundamental, second- and third-order harmonic current harmonic phasors for fault detection and location.

4 Results and Discussion

In this section, a discussion has been carried out on the performance of the RT-SHPM-FL method during various fault conditions. Numerous shunt faults with fault conditions are created randomly at different distances. This random process does include the effect of FIA on the operation of the proposed method. It emphasizes the effect of FIA on fault detection function and trained location function (SVR-FL) of the RT-SHPM-FL method because in practical scenario the occurrence of the fault w.r.t. to the current waveform is random in nature. The threshold values (k_1 & k_2) for the second- and third-order harmonic current phasors are selected as 0.1 and 0.012, respectively, after conducting numerous case studies on the experimental setup (Mallikarjua et al. 2018). The respective results are depicted in Tables 1, 2, 3, 4 and 5.

Under normal operating condition, the magnitudes of time-tagged 50, 100 and 150 Hz phasors of three-phase current signals and the operation of the proposed method are depicted in Table 1. It is clear that the values of 100 Hz and 150 Hz phasors of A, B and C current signals are 0.0006, 0.0003 & 0.0003, and 0.00015, 0.00015 & 0.00015, respectively. The proposed method has detected the present

Table 1 Performance of the proposed SVR-based fault locator

Power system condition	Time stamping (hh.mm.ss.ms on MM.DD.YY)	Fundamental, second- and third-order harmonic phasors of 3-Φ current signals			$\lvert I_{A2}\rvert > 0.1$ & $\lvert I_{A3}\rvert > 0.012$ (Y/N)	$\lvert I_{B2}\rvert > 0.1$ & $\lvert I_{B3}\rvert > 0.012$ (Y/N)	$\lvert I_{C2}\rvert > 0.1$ & $\lvert I_{C3}\rvert > 0.012$ (Y/N)	Is fault detected? (Y/N)
		$\lvert I_{A1}\rvert, \lvert I_{A2}\rvert, \lvert I_{A3}\rvert$	$\lvert I_{B1}\rvert, \lvert I_{B2}\rvert, \lvert I_{B3}\rvert$	$\lvert I_{C1}\rvert, \lvert I_{C2}\rvert, \lvert I_{C3}\rvert$				
No fault condition	2.36.47.000 PM on 06.06.2017	0.25, 0.0006, 0.00015	0.2343, 0.0003, 0.00015	0.2656, 0.0003, 0.00015	N	N	N	N

Table 2 Performance of SVR-FL for L–L–L fault with wide range of FRs at different distances

Fault condition (fault type, FR, FD)	Time stamping (hh.mm.ss.ms on MM.DD.YY)	Fundamental, second- and third-order harmonic phasors of 3-Φ current signals			$\lvert I_{A2}\rvert > 0.1$ & $\lvert I_{A3}\rvert > 0.012$ (Y/N)	$\lvert I_{B2}\rvert > 0.1$ & $\lvert I_{B3}\rvert > 0.012$ (Y/N)	$\lvert I_{C2}\rvert > 0.1$ & $\lvert I_{C3}\rvert > 0.012$ (Y/N)	Is fault detected? (Y/N)	EHPs (I_{eq1}, I_{eq2}, I_{eq3})	SVR-FL-estimated fault distance in km
		$\lvert I_{A1}\rvert, \lvert I_{A2}\rvert, \lvert I_{A3}\rvert$	$\lvert I_{B1}\rvert, \lvert I_{B2}\rvert, \lvert I_{B3}\rvert$	$\lvert I_{C1}\rvert, \lvert I_{C2}\rvert, \lvert I_{C3}\rvert$						
L–L–L, 50 Ω, 100 km	3.01.28.000 PM on 06.06.2017	0.9218, 0.125, 0.0312	0.875, 0.125, 0.0312	0.8125, 0.125, 0.0312	Y	Y	Y	Y	1.5086, 0.2692, 0.0541	101
L–L–L, 1 Ω, 150 km	3.20.38.999 PM on 06.06.2017	1.3125, 0.2969, 0.0468	1.375, 0.125, 0.0469	1.3438, 0.2813, 0.0469	Y	Y	Y	Y	2.3278, 0.4276, 0.0811	150.75
L–L–L, 0 Ω, 200 km	3.39.42.999 PM on 06.06.2017	1.125, 0.2031, 0.0313	1.0156, 0.25, 0.0469	1.1406, 0.125, 0.0313	Y	Y	Y	Y	1.8968, 0.3455, 0.0645	199.5
L–L–L, 20 Ω, 250 km	3.42.49.999 PM on 06.06.2017	0.6094, 0.181, 0.0156	0.5, 0.125, 0.0156	0.5625, 0.138, 0.0516	Y	Y	Y	Y	0.9684, 0.2596, 0.0561	252.5
L–L–L, 50 Ω, 300 km	3.56.47.000 PM on 06.06.2017	0.4219, 0.1094, 0.0156	0.4375, 0.125, 0.0156	0.4219, 0.128, 0.0156	Y	Y	Y	Y	0.7398, 0.2097, 0.027	297.6

Table 3 Performance of SVR-FL for L–L fault with wide range of FR at different distances

Fault condition (fault type, FR, FD)	Time stamping (hh.mm.ss.ms on MM.DD. YY)	Fundamental, second- and third-order harmonic phasors of 3-Φ current signals			$\lvert I_{A2}\rvert > 0.1$ & $\lvert I_{A3}\rvert > 0.012$ (Y/N)	$\lvert I_{B2}\rvert > 0.1$ & $\lvert I_{B3}\rvert > 0.012$ (Y/N)	$\lvert I_{C2}\rvert > 0.1$ & $\lvert I_{C3}\rvert > 0.012$ (Y/N)	Is fault detected? (Y/N)	EHPs (I_{eq1}, I_{eq2}, I_{eq3})	SVR-FL-estimated fault distance in km
		$\lvert I_{A1}\rvert$, $\lvert I_{A2}\rvert$, $\lvert I_{A3}\rvert$	$\lvert I_{B1}\rvert$, $\lvert I_{B2}\rvert$, $\lvert I_{B3}\rvert$	$\lvert I_{C1}\rvert$, $\lvert I_{C2}\rvert$, $\lvert I_{C3}\rvert$						
L–L, 20 Ω, 200 km	7.08.23.900 PM on 06.06.2017	0.8125, 0.1562, 0.0312	0.5937, 0.1406, 0.0312	0.2656, 0.0312, 0.0156	Y	Y	N	Y	1.0407, 0.2124, 0.0468	198
L–L, 50 Ω, 300 km	7.12.42.009 PM on 06.06.2017	0.7343, 0.1718, 0.0312,	0.625, 0.1562, 0.0312	0.2656, 0.0312, 0.0156	Y	Y	N	Y	1.0001, 0.2342, 0.0468	301.8
L–L, 5 Ω, 200 km	7.20.12.000 PM on 06.06.2017	0.3125, 0.0468, 0.0156	0.7968, 0.1875, 0.0312	0.5781, 0.1406, 0.0312	N	Y	Y	Y	1.0328, 0.2389, 0.0468	201.4
L–L, 20 Ω, 100 km	7.31.16.000 PM on 06.06.2017	0.375, 0.03125, 0.01562	1.0781, 0.2656, 0.0468	1.000, 0.25, 0.0468	N	Y	Y	Y	1.9973, 0.4585, 0.0796	99
L–L, 0 Ω, 50 km	7.32.19.120 PM on 06.06.2017	3.125, 0.7187, 0.1406	0.25, 0.0625, 0.0156	3.2968, 0.7812, 0.1406	Y	N	Y	Y	4.5493, 1.0633, 0.1994	49.8
L–L, 1 Ω, 150 km	7.33.46.000 PM on 06.06.2017	1.109, 0.234, 0.0468	0.25, 0.0625, 0.0156	1.296, 0.296, 0.0625	Y	N	Y	Y	1.7239, 0.3824, 0.0796	149.445

Table 4 Performance of SVR-FL for L–LG fault with wide range of FR at different distances

Fault condition (fault type, FR, FD)	Time stamping (hh.mm.ss.ms on MM.DD. YY)	Fundamental, second- and third-order harmonic phasors of 3-Φ current signals			$\lvert I_{A2}\rvert > 0.1$ & $\lvert I_{A3}\rvert > 0.012$ (Y/N)	$\lvert I_{B2}\rvert > 0.1$ & $\lvert I_{B3}\rvert > 0.012$ (Y/N)	$\lvert I_{C2}\rvert > 0.1$ & $\lvert I_{C3}\rvert > 0.012$ (Y/N)	Is fault detected? (Y/N)	EHPs (I_{eq1}, I_{eq2}, I_{eq3})	SVR-FL-estimated fault distance in km
		$\lvert I_{A1}\rvert$, $\lvert I_{A2}\rvert$, $\lvert I_{A3}\rvert$	$\lvert I_{B1}\rvert$, $\lvert I_{B2}\rvert$, $\lvert I_{B3}\rvert$	$\lvert I_{C1}\rvert$, $\lvert I_{C2}\rvert$, $\lvert I_{C3}\rvert$						
L–LG, 20 Ω, 300 km	7.34.13.120 PM on 06.06.2017	0.625, 0.125, 0.0312	0.4675, 0.102, 0.0156	0.25, 0.043, 0.012	Y	Y	N	Y	0.8195, 0.1669, 0.0368	297.33
L–LG, 5 Ω, 150 km	7.35.21.998 PM on 06.06.2017	1.531, 0.343, 0.165	1.18, 0.14, 0.0312	0.25, 0.062, 0.0156	Y	Y	N	Y	1.9331, 0.3756, 0.1686	148.965
L–LG, 50 Ω, 250 km	7.36.02.097 PM on 06.06.2017	0.4062, 0.0625, 0.0156	1.0, 0.25, 0.0468	0.7968, 0.1875 0.0312	N	Y	Y	Y	1.3416, 0.3186, 0.0584	249.23
L–LG, 0 Ω, 50 km	7.37.00.099 PM on 06.06.2017	0.2968, 0.0625, 0.0156	4.09, 0.7343, 0.0146	3.78, 0.4067, 0.093	N	Y	Y	Y	5.5771, 0.8417, 0.0954	49.124
L–LG, 50 Ω, 200 km	7.37.06.000 PM on 06.06.2017	0.8125, 0.125, 0.03125	0.2656, 0.0625, 0.0156	0.9531, 0.1718, 0.03125	Y	N	Y	Y	1.2803, 0.2215, 0.0468	202
L–LG, 1 Ω, 100 km	7.38.42.150 PM on 06.06.2017	1.6719, 0.4063, 0.0781	0.2344, 0.0469, 0.0156	2.0625, 0.3906, 0.0781	Y	N	Y	Y	2.6653, 0.5655, 0.1115	99.65

Table 5 Performance of SVR-FL for LG fault with wide range of FR at different distances

Fault condition (fault type, FR, FD)	Time stamping (hh.mm.ss.ms on MM.DD.YY)	Fundamental, second- and third-order harmonic phasors of 3-Φ current signals			$\lvert I_{A2}\rvert > 0.1$ & $\lvert I_{A3}\rvert > 0.012$ (Y/N)	$\lvert I_{B2}\rvert > 0.1$ & $\lvert I_{B3}\rvert > 0.012$ (Y/N)	$\lvert I_{C2}\rvert > 0.1$ & $\lvert I_{C3}\rvert > 0.012$ (Y/N)	Is fault detected? (Y/N)	EHPs (I_{eq1}, I_{eq2}, I_{eq3})	SVR-FL-estimated fault distance in km
		$\lvert I_{A1}\rvert, \lvert I_{A2}\rvert, \lvert I_{A3}\rvert$	$\lvert I_{B1}\rvert, \lvert I_{B2}\rvert, \lvert I_{B3}\rvert$	$\lvert I_{C1}\rvert, \lvert I_{C2}\rvert, \lvert I_{C3}\rvert$						
LG, 0 Ω, 50 km	7.38.59.000 PM on 06.06.2017	3.5625, 0.7968, 0.1406	0.2656, 0.0468, 0.0156	0.2343, 0.0468, 0.0156	Y	–	–	Y	3.58007, 0.7996, 0.1423	49.512
LG, 1 Ω, 100 km	7.42.35.150 PM on 06.06.2017	2.062, 0.25, 0.0625	0.25, 0.0625, 0.0156	0.2656, 0.0312, 0.0156	Y	–	–	Y	2.094, 0.2596, 0.0665	99.5
LG, 20 Ω, 300 km	7.51.25.978 PM on 06.06.2017	0.2812, 0.0625, 0.0156	0.5, 0.125, 0.0156	0.2656, 0.0312, 0.0156	N	Y	–	Y	0.6322, 0.1432, 0.02701	297
LG, 5 Ω, 250 km	7.56.06.998 PM on 06.06.2017	0.3125, 0.0468, 0.0156	0.25, 0.0625, 0.0156	0.75, 0.1718, 0.0312	N	N	Y	Y	0.8501, 0.1887, 0.0382	248.75
LG, 50 Ω, 50 km	8.12.42.000 PM on 06.06.2017	0.2968, 0.0468, 0.0156	0.2812, 0.0312, 0.0156	0.5625, 0.14, 0.0156	N	N	Y	Y	0.6354, 0.1509, 0.027	50.5

condition as 'No Fault' since the magnitude of neither synchronized 100 Hz & 150 Hz current phasors nor 50 Hz phasor are/is greater than the respective set value(s). This situation is depicted in Fig. 4.

The performance of the RT-SHPM-FL method for different fault conditions along with the corresponding results is depicted in Tables 2, 3, 4 and 5. For instance, consider a triple-line fault (L–L–L) with FR of 50 Ω at 100 km. The synchronized harmonic phasor measurements of three-phase currents are tabulated in Table 2. The time-stamped 100 and 150 Hz current phasors in ampere are ($I_{A2} = 0.125$, $I_{B2} = 0.125$ & $I_{C2} = 0.125$) and ($I_{A3} = 0.03125$, $I_{B3} = 0.03125$ & $I_{C3} = 0.03125$), respectively. When these values are transferred to the proposed method, the fault is detected since the 100 and 150 Hz current phasors are higher than the respective set values. The EHPs calculated from the 50, 100 and 150 Hz three-phase current phasors are also given in Table 2. When the respective EHPs ($|I_{eq1}| = 1.5086$, $|I_{eq2}| = 0.2692$ & $|I_{eq3}| = 0.0541$) are passed through the trained SVR-FL, the estimated fault distance is 101 km. Similarly, the performance of RT-SHPM-FL method has been validated for L–L–L fault with wide-range variation in fault conditions as tabulated in Table 2.

Further, different double-line faults (L–L) with distinct FRs are created at different distances, and the corresponding results are tabulated in Table 3. For example, consider an L-L fault at 100 km with FR of 20 Ω from the source end. The time-stamped 100 and 150 Hz three-phase current phasors' magnitudes estimated at 7.31.16.000 PM on 06.06.2017 are (0.03125, 0.2656 & 0.25) and (0.0156, 0.0468 & 0.0468) respectively. When these values are passed through the RT-SHPM-FL method, the fault has been detected. The fault distance estimated by trained SVR-FL using the respective EHPs is 99 km. This condition is shown in Fig. 5. Likewise, different L–L faults with wide-range variation in FR and FD are detected and located by the proposed method, which are given in Table 3.

As given in Table 4, furthermore the double-line-to-ground fault (L–LG) with distinct values of FR is created randomly at different distances. For a case in point, consider an L–LG with 50 Ω occurred at 200 km from the source end. When the resultant time-stamped magnitudes of 100 and 150 Hz current phasors measured at 7.37.06.000 PM on 06.06.2017 are passed through the proposed fault location method, the fault is detected as shown in Table 4. The trained SVR-FL estimated the C–AG fault distance as 202 km from the source end. Similarly, as given in Table 4, the proposed fault location method has detected and located the L–LG fault with different fault conditions.

Likewise, the estimated values of time-stamped 100 and 150 Hz of three-phase current phasors for line-to-ground (LG) fault with distinct FRs at various distances are depicted in Table 5. For example, assume an LG fault with FR of 0

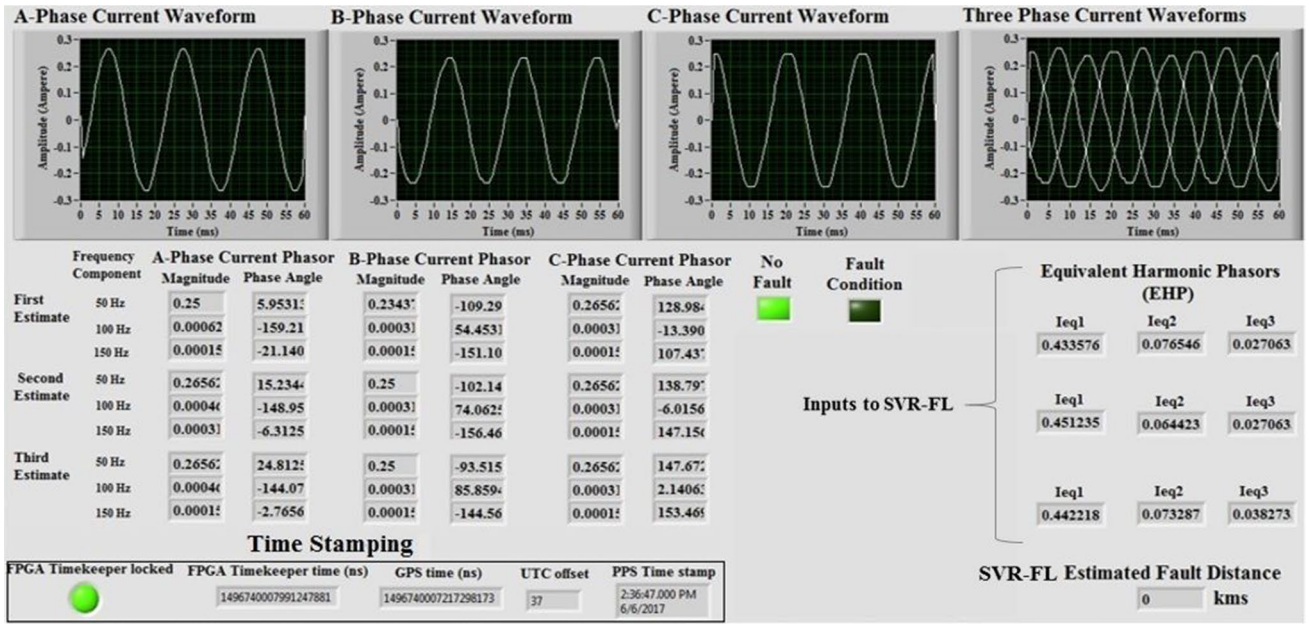

Fig. 4 LabVIEW front panel display for no fault condition

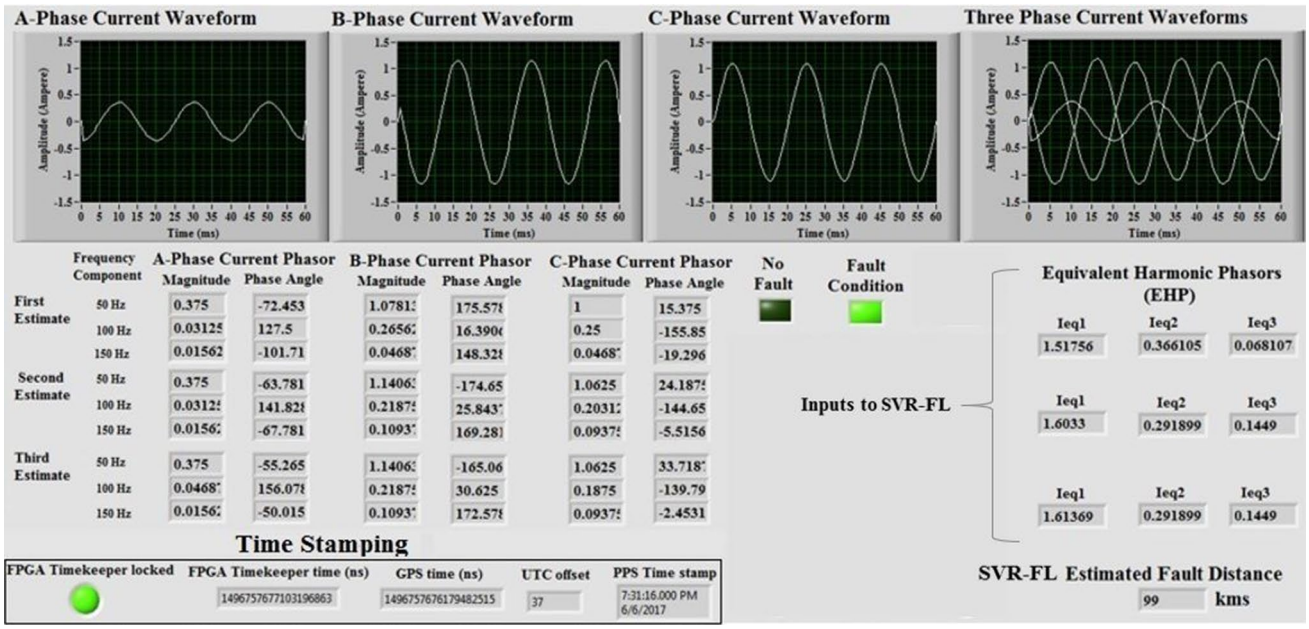

Fig. 5 LabVIEW front panel display for L–L fault with FR = 20 Ω at 100 km from the source end (Bus 1)

Ω has occurred at 50 km from the source end. The time-stamped magnitudes of 100 Hz ($I_{A2}, I_{B2}\&I_{C2}$) and 150 Hz ($I_{A3}, I_{B3}\&I_{C3}$) phasors of three-phase current signals estimated at 7.38.59.000 PM on 06.06.2017 are (0.7968, 0.0468 & 0.0468) and (0.1406, 0.0156 & 0.0156), respectively. When the EHPs of synchronized harmonic current phasors are passed through the proposed fault location method, it recognized the prevailing condition as a fault since 100 and 150 Hz current phasors are greater than 0.1 and 0.012, respectively. Furthermore, LG fault with different fault conditions is detected and located as depicted in Table 5.

From the elaborated discussions carried above, the fault detection and location functions of RT-SHPM-FL method have detected the faults precisely and located the faults with

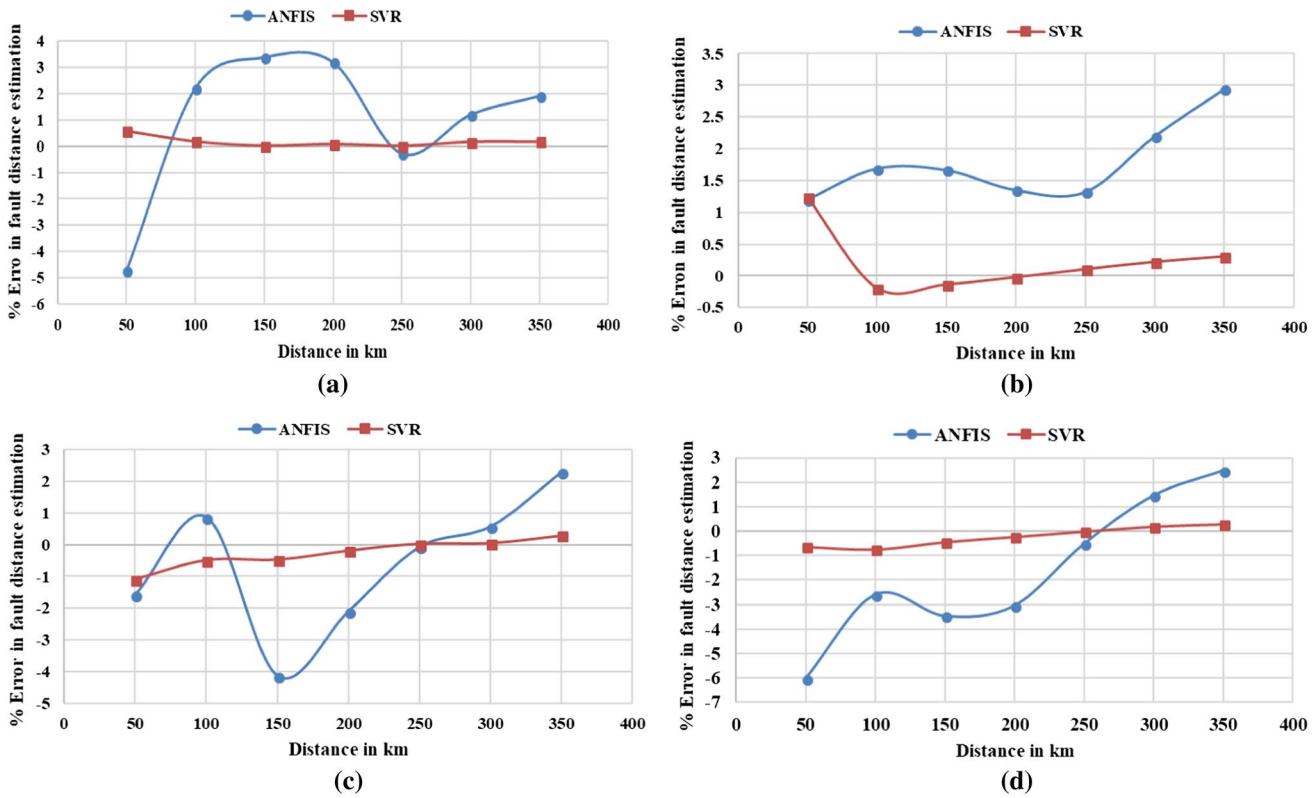

Fig. 6 Percentage error in fault distance estimation in real time, **a** when L–L–L fault with FR = 20 Ω occurred; **b** when L–LG fault with FR = 0 Ω occurred; **c** when L–L fault with FR = 1 Ω occurred; and **d** when LG fault with FR = 5 Ω occurred

less error. Also, the user-friendly interface shows its suitability of the proposed RT-SHPM-FL method for real-time applications. In the following section, a comparative analysis is carried out to show the superiority of SVR-FL over ANFIS-based fault location as described below.

5 Comparative Analysis of SVR-Based Fault Locator and ANFIS-Based Fault Locator

Once a fault is detected, EHPs are calculated from 50, 100 and 150 Hz three-phase current phasors corresponding to the fault conditions. SVR and ANFIS are trained with these EHPs and fault distance as inputs and output, respectively. The accuracy of the proposed method using SVR in fault location is superior over that of ANFIS. Fuzzy inference system in ANFIS classifier is trained using a hybrid optimization method (Gaussian combination membership function) (Hsu and Lin 2002). The ANFIS classifier comprises of 181 membership functions. The training set contains 1400 samples, and each type of fault contains 140 samples. Figure 6 shows the percentage error in fault distance estimation by the proposed method using SVR and ANFIS. From Fig. 6a–d, it is evident that the percentage error in fault location is within ± 1% using SVR while using ANFIS varies widely with different fault conditions.

6 Conclusions

This paper proposes a RT-SHPM-FL method for fault location in transmission lines using SVR. The synchronized harmonic phasor measurements of three-phase current signals obtained from PMUs are used to detect a fault. Also, the fault distance is estimated using magnitudes of EHPs. For fault distance estimation in transmission lines, the RT-SHPM-FL method has employed SVR. The fault detection and location functions (SVR-FL) of the RT-SHPM-FL method are implemented in LabVIEW software. The proposed method has been tested on a scaled-down laboratory model of 400 kV EHV transmission line of 400 km long. The results show that the proposed method using SVR for fault location has been superior over ANFIS since the error associated with the former one is less than ± 1% regardless of the fault conditions.

Acknowledgements The authors would like to thank the Science and Engineering Research Board (SERB), Department of Science and Technology (DST), India for financially supporting this work through the sanction order no. CRG/2018/000302 and EMR/2017/001508.

References

Barman, S., & Roy, B. K. S. (2018). Detection and location of faults in large transmission networks using minimum number of phasor measurement units. *IET Generation, Transmission and Distribution, 12*(8), 1941–1950. https://doi.org/10.1049/iet-gtd.2017.1067.

Chang, C. C., & Lin, C.-J. (2011). LIBSVM: A library for support vector machines. *ACM Transactions on Intelligent Systems and Technology, 2,* 27:1–27:27.

Das, S., Singh, S. P., & Panigrahi, B. K. (2017). Transmission line fault detection and location using Wide Area Measurements. *Electric Power Systems Research, 151,* 96–105. https://doi.org/10.1016/j.epsr.2017.05.025.

Fei, C., Qi, G., & Li, C. (2018). Fault location on high voltage transmission line by applying support vector regression with fault signal amplitudes. *Electric Power Systems Research, 160,* 173–179.

Gao, F., Thrp, J. S., Gao, S., Pal, A., & Vance, K. A. (2015). A voltage phasor based fault-classification method for phasor measurement unit only state estimator output. *Electric Power Components and Systems, 43*(1), 22–31.

Gopakumar, P., Jaya Bharata Reddy, M., & Mohanta, D. K. (2015). Fault detection and localization methodology for self-healing in smart power grids incorporating phasor measurement units. *Electric Power Components and Systems, 43*(6), 695–710.

Hsu, C. W., & Lin, C. J. (2002). A comparison of methods for multiclass support vector machines. *IEEE Transactions on Neural Networks, 13*(2), 415–425.

IEEE Standard for Synchrophasor Data Transfer for Power Systems. IEEE Standard C37.118.2-2011 (revision of IEEE Std C37.118-2005), 1–53.

Jaya Bharata Reddy, M., Gopakumar, P., & Mohanta, D. K. (2016). A novel transmission line protection using DOST and SVM. *International Journal on Engineering Science and Technology, 19*(2), 1027–1039.

Jiang, Z., Miao, S., Xu, H., Liu, P., & Zhang, B. (2012). An effective fault location technique for transmission grids using phasor measurement units. *International Journal of Electrical Power & Energy Systems, 42*(1), 653–660. https://doi.org/10.1016/j.ijepes.2012.03.020.

Kang, N., Gombos, G., Mousavi, M. J., & Feng, X. (2017). A fault location algorithm for two-end series-compensated double-circuit transmission lines using the distributed parameter line model. *Electric Power Components and Systems, 45*(6), 615–623.

Kumar, G. R., Gafoor, S. A., & Ram, S. S. T. (2015). A transient current based double line transmission system protection using fuzzy-wavelet approach in the presence of UPFC. *International Journal of Electrical Power & Energy Systems, 70,* 91–98.

Mallikarjua, B., Chatterjee, D., Jaya Bharata Reddy, M., & Mohanta, D. K. (2018). Real-time wide-area disturbance monitoring and protection methodology for EHV transmission lines. *INAE Letters, 3*(2), 87–106. https://doi.org/10.1007/s41403-018-0038-z.

Manassero Junior, G., Santo, S. G. D., & Rojas, D. G. (2016). Fault location in series-compensated transmission lines based on heuristic method. *Electric Power Systems Research, 140,* 950–957. https://doi.org/10.1016/j.epsr.2016.03.049.

Meenakshi Devi, M., Geethanjali, M., & Rama Devi, A. (2018). Fault localization for transmission lines with optimal phasor measurement units. *Computers and Electrical Engineering*. https://doi.org/10.1016/j.compeleceng.2018.01.043.

Mousavi-Seyedi, S. S., Aminifar, F., Rezaei, M. R., & Hasani, R. (2015). Optimal fault location algorithm for series-compensated transmission lines based on PMU data. In *Smart grid conference (SGC), Tehran*, pp. 105–109. https://doi.org/10.1109/sgc.2015.7857418.

Pasand, M. S., & Malik, O. P. (1999). Implementation & laboratory test results of an Elman network-based transmission line directional relay. *IEEE Transactions on Power Delivery, 14*(3), 782–788.

Rajaraman, P., Sundaravaradan, N. A., Mallikarjuna, B., Jaya Bharata Reddy, M., & Mohanta, D. K. (2018). Robust fault analysis in transmission lines using synchrophasor measurements. *Protection and Control of Modern Power Systems, 14*(3), 1–13.

Roy, N., & Bhattacharya, K. (2015). Detection, classification, and estimation of fault location on an overhead transmission line using S-transform and neural network. *Electric Power Components and Systems, 43*(4), 461–472.

Saber, A. (2018). New fault location scheme for four-circuit untransposed transmission lines. *International Journal of Electrical Power & Energy Systems, 99,* 225–232. https://doi.org/10.1016/j.ijepes.2018.01.006.

Software available at http://www.csie.ntu.edu.tw/~cjlin/libsvm.

Vallapu, P. P., Moradi-Pari, E., Fallah, Y. P., & Famouri, P. (2017). Detection and location of faults in wide area systems utilizing event-based communication scheduling. In *North American Power Symposium (NAPS), Morgantown, WV*, pp. 1–6. https://doi.org/10.1109/naps.2017.8107396.

Vapnik, V. (1998). *Statistical learning theory* (p. 1998). New York: Wiley.

Vapnik, V., Golowich, S., & Smola, A. (1997). Support vector method for function approximation, regression estimation, and signal processing. *Advances in Neural Information Processing Systems, 9,* 281–287.

Venkatesan, R., & Balamurugan, B. (2001). A real-time hardware fault detector using an artificial neural network for distance protection. *IEEE Transactions on Power Delivery, 16*(1), 75–82.

Yusuff, A. A., Jimoh, A. A., & Munda, J. L. (2014). Fault location in transmission lines based on stationary wavelet transform, determinant function feature and support vector regression. *Electric Power Systems Research, 110,* 73–83.